AIAA JOURNAL
Vol. 34, No. 7, July 1996

Implicit Computation of Three-Dimensional Compressible Navier–Stokes Equations Using k–ε Closure

G. A. Gerolymos* and I. Vallet†
Université Pierre-et-Marie-Curie, 91405 Orsay, Paris, France

A computational method for the numerical integration of the Favre–Reynolds-averaged three-dimensional compressible Navier–Stokes equations using the Launder–Sharma near-wall k–ε turbulence closure is developed. The mean flow and turbulence transport equations are discretized using a finite volume method based on MUSCL Van Leer flux-vector splitting with Van Albada limiters. The mean flow and turbulence equations are integrated in time using a fully coupled approximately factored implicit backward Euler method. The resulting scheme is robust and was found stable for local-time steps with Courant–Friedrichs–Lewy number equal to 50. Higher time steps are possible but not optimal for convergence. Results are presented for the three Délery transonic channel test-cases. Although these test-cases are nominally two dimensional, three-dimensional computations presented quantify the important three-dimensional effects induced by the sidewall boundary layers. Finally computational results are compared with the experiment for a geometrically three-dimensional transonic nozzle.

Introduction

NEAR-WALL two-equation turbulence models[1–8] are increasingly used in computational fluid dynamics (CFD), and it is hoped that some of their modeling drawbacks will be corrected by the use of more advanced models[9–11] including near-wall Reynolds-stress models[12–16] and compressibility effects.[17–21] The interest in using transport-equation models of turbulence in CFD is the result not only of their higher accuracy in complex configurations but also of the simpler computer logic involved with comparison to zero-equation models. The authors believe that near-wall turbulence models are more interesting for CFD purposes than the wall-functions approach, although opinion on this is divided.[22–24]

The major problem of codes using transport-equation models of turbulence in the transonic regime (including shock-wave/boundary-layer interaction) is their robustness and, as a consequence, their computational efficiency. A satisfactory method should run from a simple automatic initialization of the flowfield and have the same convergence characteristics, in terms of Courant–Friedrichs–Lewy (CFL) number[25] (time marching schemes) or relaxation parameters (pressure-based schemes and Newton-iteration procedures), as their zero-equation model counterparts, as well as exhibit robustness characteristics analogous to zero-equation model methods. The last point is a major item and, if achieved, transport-equation models will presumably definitely replace zero-equation models, at least for complex three-dimensional configurations where the implementation of models using such concepts as distance from the wall and profile extremum is delicate.

This work is not concerned so much with turbulence modeling as with the efficient numerical implementation of low-Reynolds near-wall two-equation models. An overview of methods using two-equation models in the transonic regime, including a summary of their computational characteristics, is interesting (Table 1).[26–77] This overview is certainly not exhaustive and is mostly based on *AIAA Journal* articles, but the authors believe it is quite representative of the evolution of the state of the art over the past 10 years. The nondimensional distance from the wall of the first grid point nearest to it, $n_w^+ = n\nu_w^{-1}\sqrt{(|\tau_w|\rho_w^{-1})}$ (where n is the distance from the wall, τ_w the resultant wall shear stress, ρ_w the density at the wall, and ν_w the kinematic viscosity at the wall), is a very important grid-resolution parameter. Most workers (Table 1) acknowledge that, in the transonic régime ($M < 2$?), values of $n_w^+ < 1$ are necessary to obtain accurate grid-independent results.

Practically all methods can be augmented by a multigrid procedure to achieve higher computational efficiency.[43,49–52] Independent of this, the admissible CFL number is an approximate gauge of the computational rapidity of time-marching methods. This is not true for relaxation methods where time does not appear explicitly, nor for the hybrid MacCormack scheme. Neither of these methods can be readily extended to unsteady flows. When time-marching methods are considered, it appears that the average CFL number used is ~5 (Table 1). Increasing the optimal CFL number has a nonlinear accelerating effect on convergence and is, therefore, highly desirable. Unsteady flow computations consistently use much higher CFL numbers that are stable in the highly stretched grids used without local time-stepping (for consistency), and will not be considered here.[78–82] There are three published methods that appear more advanced than the others. Coakley[30] and Lin et al.[58] achieved CFL = 8 using upwind discretizations with implicit approximate factorization. Lin et al.[58] achieved CFL = 70 using a nonfactored implicit method, but the cost/iteration is about three times greater than factored methods. A more important problem of nonfactored methods is that computer-memory-requirements are 1 order of magnitude greater (compared with factored methods in three-dimensions).

There are, unfortunately, few authors who analyze the problems associated with the numerical implementation of two-equation models. The use of limiters was introduced by Coakley and Viegas,[27] who used minimum bounds and a maximum–minimum turbulence length-scale concept to ensure positivity and boundedness of turbulence variables (k, ε, or ω). Other authors[43,45,46,51,52,57] used analogous limiters, often also limiting the production of turbulence kinetic energy P_k with respect to its dissipation ε to avoid nonphysical overshoots in the neighborhood of the shock wave. One of the few systematic attempts to analyze the stability of k–ε solvers was reported by Kunz and Lakshminarayana.[46] There seems to be some doubt concerning whether source terms are stiff or not, what their importance on stability is, and whether their implicit treatment is necessary, different authors reporting contradictory conclusions. There is not necessarily a unique answer to these questions, since the interaction between the numerical scheme, the limiters, and the model should be considered as an integrated system and not separately. A review of the literature and practical experience tend to point out that (although the authors are unable to prove this mathematically) upwind schemes are more robust for treating the convection of turbulence variables; limiters are most important at the boundary-layer edge, where production and dissipation decrease

Received Sept. 1, 1995; revision received Jan. 12, 1996; accepted for publication Jan. 22, 1996.

*Professor, Director, Laboratoire d'Energétique, Unité de Recherche Associée au Centre National de la Recherche Scientifique 1504, Building 511.

†Ministry of Scientific Research Research Assistant, Unité de Recherche Associée au Centre National de la Recherche Scientifique 1504, Building 511.

Table 1 Time-marching methods for transonic Navier–Stokes with two-equation closure and local-time-stepping

References	Date	Two/three dimensional	Model (Ref.)	Space	Time	CFL	n_w^+
27–29	1977	Two dimensional	k–ε(3)	MacCormack[59]	Hybrid[59]	—	5
30	1985	Two dimensional	q–ω(7)	Coakley[30]	SR[a] implicit[30]	5–8	0.8
31	1986	Two dimensional	k–ε(3)	MacCormack[59]	Hybrid[59]	—	?
32–34	1986	Three dimensional	k–ε(3)	MacCormack[59]	Explicit[59]	<1	WF[b]
35–38	1986	Three dimensional	k–ε(3)	MacCormack[59]	Hybrid[59]	—	0.3–0.7
39	1986	Two dimensional	k–ε(6)	Beam–Warming[60]	AF[c] implicit	?	1
40	1988	Two dimensional	k–ε(26)	Hopscotch[62]	Explicit[61]	<1	WF
41	1989	Three dimensional	q–ω(7)	Coakley[30]	SR implicit[30]	3–5	1
42	1990	Three dimensional	k–ε(26)	Jameson[63]	SR implicit[42]	4–6	WF
43	1990	Two dimensional	k–ε(5)	Ni[65]	SR implicit[66]	3	0.2
44	1991	Two dimensional	k–ε(6)	Quick[64]	PB[d 44]	—	1–5
45	1992	Two dimensional	k–ε(6)	Jameson[63]	Explicit RK[e 63]	$2\sqrt{2}$	1
46	1992	Three dimensional	k–ε(6)	Jameson[63]	Explicit RK[63]	$2\sqrt{2}$	1
47	1992	Two dimensional	k–ε(5)	MacCormack[59]	Explicit[59]	0.4–0.8	1
48	1992	Two dimensional	q–ω(7)	Jameson[63]	SR implicit[30,60]	5?	1
49	1993	Two dimensional	k–ε	Ni[65]	Explicit[65]	<1	1
50	1993	Two dimensional	k–ε(50)	Quick[67]	Explicit PB[50]	<1?	1
51, 52	1993	Three dimensional	k–ε	Jameson[63]	Explicit RK[63]	$2\sqrt{2}$	WF
53	1994	Three dimensional	k–ε(5)	Beam–Warming[60]	AF implicit[60]	5	1
54	1994	Two dimensional	k–ε(8)	Liu and Jameson[68]	Explicit RK[63]	5?	0.5–2
55	1995	Three dimensional	k–ε(3)	Lax-Wendroff[69]	Explicit[63]	<1	3
56	1995	Two dimensional	k–ε(8)	Roe[70,71]	Explicit RK63	3?	0.5–2
57	1995	Three dimensional	k–ε(26)	unstructured[57] Roe	SR implicit[63,72]	2	WF
58	1995	Two dimensional	k–ε(6)	Yee–Harten[73]	AF implicit[58]	8?	0.55
58	1995	Two dimensional	k–ε(6)	Yee–Harten[73]	NF[f] implicit[58]	70?	0.55
Present	1996	Three dimensional	k–ε(5)	Van Leer[74,75]	AF implicit[76,77]	50	0.5

[a]SR = spectral radius. [b]WF = wall functions. [c]AF = approximately factored. [d]PB = pressure based. [e]RK = Runge–Kutta. [f]NF = nonfactored.

rapidly, and diffusion balances convection (an interesting analysis of the associated instability is given by Stüttgen and Peters[83]), and not, as is often stated by wall-function users, in the near-wall region; and the importance of the implicit treatment of source terms depends strongly on the scheme used.

The purpose of this work is to develop a fully coupled implicit upwind scheme for the three-dimensional compressible Navier–Stokes equations, combining computational efficiency and computational robustness. The method is based on Van Leer MUSCL discretization[74,75] of the convective terms, with factored implicit time integration.[76,77] The Jacobian operator of the implicit step is approximated by a first-order upwind scheme for the convective fluxes, and a spectral-radius matrix for the viscous fluxes. The source-terms are simply factored, without using any special procedure, such as suggested by Shih and Chyu,[84] or positivity fixes.[31] Optimal convergence is obtained for CFL = 50. The method is applied to the computation of several transonic channel flows.

Flow Model and Computational Method

Flow Model

The flow is modeled by the compressible Favre–Reynolds-averaged[85,86] three-dimensional Navier–Stokes equations, with a compressible flow extension to the Launder–Sharma[5] near-wall k–ε closure:

$$\frac{\partial \bar\rho}{\partial t} + \frac{\partial \bar\rho \tilde u_j}{\partial x_j} = 0 \tag{1}$$

$$\frac{\partial \bar\rho \tilde u_i}{\partial t} + \frac{\partial}{\partial x_j}[\bar\rho \tilde u_i \tilde u_j + \bar p \delta_{ij}] - \frac{\partial(\bar\tau_{ij} - \overline{\rho u_i'' u_j''})}{\partial x_j} = 0 \tag{2}$$

$$\frac{\partial(\bar\rho \breve h_t - \bar p)}{\partial t} + \frac{\partial \bar\rho \tilde u_j \breve h_t}{\partial x_j} - \frac{\partial}{\partial x_j}[\tilde u_i(\bar\tau_{ij} - \overline{\rho u_i'' u_j''}) - (\bar q_j + \overline{\rho e'' u_j''})] + P_k - \bar\rho\varepsilon^* - 2\mu \frac{\partial\sqrt{k}}{\partial x_j}\frac{\partial\sqrt{k}}{\partial x_j} = 0 \tag{3}$$

$$\frac{\partial \bar\rho k}{\partial t} + \frac{\partial \bar\rho \tilde u_j k}{\partial x_j} - \frac{\partial}{\partial x_j}\left[\left(\mu + \frac{\mu_T}{\sigma_k}\right)\frac{\partial k}{\partial x_j}\right] - P_k + \bar\rho\varepsilon^* + 2\mu\frac{\partial\sqrt{k}}{\partial x_j}\frac{\partial\sqrt{k}}{\partial x_j} = 0 \tag{4}$$

$$\frac{\partial \bar\rho\varepsilon^*}{\partial t} + \frac{\partial \bar\rho \tilde u_j \varepsilon^*}{\partial x_j} - \frac{\partial}{\partial x_j}\left[\left(\mu + \frac{\mu_T}{\sigma_\varepsilon}\right)\frac{\partial \varepsilon^*}{\partial x_j}\right] - C_{\varepsilon 1} P_k \frac{\varepsilon^*}{k} + C_{\varepsilon 2} f_{\varepsilon 2}\bar\rho\frac{\varepsilon^{*2}}{k} - 2\frac{\mu\mu_T}{\bar\rho}\left(\frac{\partial^2 \tilde u_i}{\partial x_j \partial x_j}\right)\left(\frac{\partial^2 \tilde u_i}{\partial x_\ell \partial x_\ell}\right) = 0 \tag{5}$$

$$\bar p = \bar\rho R_g \tilde T = \bar\rho \tfrac{\gamma-1}{\gamma}\tilde h = \bar\rho(\gamma - 1)\tilde e$$
$$-\overline{\rho u_i'' u_j''} = \mu_T\left[\frac{\partial \tilde u_i}{\partial x_j} + \frac{\partial \tilde u_j}{\partial x_i}\right] - \frac{2}{3}\mu_T\frac{\partial \tilde u_j}{\partial x_j}\delta_{ij} - \frac{2}{3}\bar\rho k \delta_{ij} \tag{6}$$
$$\bar\tau_{ij} \cong \mu(\tilde T)\left[\frac{\partial \tilde u_i}{\partial x_j} + \frac{\partial \tilde u_j}{\partial x_i}\right] - \frac{2}{3}\mu\frac{\partial \tilde u_j}{\partial x_j}\delta_{ij}$$

$$P_k = -\frac{1}{2}\overline{\rho u_i'' u_j''}\left[\frac{\partial \tilde u_i}{\partial x_j} + \frac{\partial \tilde u_j}{\partial x_i}\right]; \qquad \bar q_i \cong -\kappa(\tilde T)\frac{\partial \tilde T}{\partial x_i} \tag{7}$$
$$\overline{\rho e'' u_j''} = -\kappa_T\frac{\partial \tilde T}{\partial x_i}$$

where t is the time, x_i the Cartesian space coordinates, $\tilde u_i$ the velocity components, $\bar\rho$ the density, $\bar p$ the pressure, $\tilde T$ the temperature, $\tilde h$ the enthalpy, $\gamma = 1.4$ the isentropic exponent, $R_g = 287.04\ \mathrm{m^2\ s^{-2}\ K^{-1}}$ the gas constant for air, $\breve h_t = \tilde h + \frac{1}{2}\tilde u_i \tilde u_i$ the total enthalpy of the mean flow (which is different from $\tilde h_t = \breve h_t + k$), k the turbulence kinetic energy, ε^* the isotropic part of the turbulence-kinetic-energy dissipation rate ($\varepsilon^* \doteq \varepsilon - 2\nu[\mathrm{grad}\sqrt{k}]^2$, where ε is the dissipation rate, and ν the kinematic viscosity), $\bar\tau_{ij}$ the viscous stress tensor, μ the molecular dynamic viscosity, μ_T the eddy viscosity, κ the molecular heat conductivity, and κ_T the eddy heat conductivity; $\tilde{\ }$ denotes Favre averaging, and $\bar{\ }$ denotes nonweighted averaging. The near-wall terms, accounting for the anisotropic part of the dissipation rate, in the k equation ($2\mu[\mathrm{grad}\sqrt{k}]^2$) and in the ε equation ($2\nu\mu_T[\nabla^2\tilde V]^2$), are written in Cartesian tensor form, independently of the wall distance or orientation.[2,43,45] The model constants and the molecular diffusion coefficients are

$$C_{\varepsilon 1} = 1.44; \quad C_{\varepsilon 2} = 1.92; \quad \sigma_k = 1; \quad \sigma_\varepsilon = 1.3$$
$$f_{\varepsilon 2}(Re_T) = 1 - 0.3e^{-Re_T^2}; \quad Re_T \doteq k^2/\nu\varepsilon^* \tag{8}$$

$$\frac{\mathrm{d}w_{i,j,k}}{\mathrm{d}t} \cong -\frac{1}{\mathcal{V}_{i,j,k}}\left[\begin{array}{l} +^{\xi}\mathcal{S}_{i+\frac{1}{2},j,k}\left[F^{+}\left({}^{\xi}w^{-}_{i+\frac{1}{2},j,k},{}^{\xi}n_{i+\frac{1}{2},j,k}\right)+F^{-}\left({}^{\xi}w^{+}_{i+\frac{1}{2},j,k},{}^{\xi}n_{i+\frac{1}{2},j,k}\right)+{}^{V}F_{i+\frac{1}{2},j,k}\cdot{}^{\xi}n_{i+\frac{1}{2},j,k}\right]\\ -^{\xi}\mathcal{S}_{i-\frac{1}{2},j,k}\left[F^{+}\left({}^{\xi}w^{-}_{i-\frac{1}{2},j,k},{}^{\xi}n_{i-\frac{1}{2},j,k}\right)+F^{-}\left({}^{\xi}w^{+}_{i-\frac{1}{2},j,k},{}^{\xi}n_{i-\frac{1}{2},j,k}\right)+{}^{V}F_{i-\frac{1}{2},j,k}\cdot{}^{\xi}n_{i-\frac{1}{2},j,k}\right]\\ +^{\eta}\mathcal{S}_{i,j+\frac{1}{2},k}\left[F^{+}\left({}^{\eta}w^{-}_{i,j+\frac{1}{2},k},{}^{\eta}n_{i,j+\frac{1}{2},k}\right)+F^{-}\left({}^{\eta}w^{+}_{i,j+\frac{1}{2},k},{}^{\eta}n_{i,j+\frac{1}{2},k}\right)+{}^{V}F_{i,j+\frac{1}{2},k}\cdot{}^{\eta}n_{i,j+\frac{1}{2},k}\right]\\ -^{\eta}\mathcal{S}_{i,j-\frac{1}{2},k}\left[F^{+}\left({}^{\eta}w^{-}_{i,j-\frac{1}{2},k},{}^{\eta}n_{i,j-\frac{1}{2},k}\right)+F^{-}\left({}^{\eta}w^{+}_{i,j-\frac{1}{2},k},{}^{\eta}n_{i,j-\frac{1}{2},k}\right)+{}^{V}F_{i,j-\frac{1}{2},k}\cdot{}^{\eta}n_{i,j-\frac{1}{2},k}\right]\\ +^{\zeta}\mathcal{S}_{i,j,k+\frac{1}{2}}\left[F^{+}\left({}^{\zeta}w^{-}_{i,j,k+\frac{1}{2}},{}^{\zeta}n_{i,j,k+\frac{1}{2}}\right)+F^{-}\left({}^{\zeta}w^{+}_{i,j,k+\frac{1}{2}},{}^{\zeta}n_{i,j,k+\frac{1}{2}}\right)+{}^{V}F_{i,j,k+\frac{1}{2}}\cdot{}^{\zeta}n_{i,j,k+\frac{1}{2}}\right]\\ -^{\zeta}\mathcal{S}_{i,j,k-\frac{1}{2}}\left[F^{+}\left({}^{\zeta}w^{-}_{i,j,k-\frac{1}{2}},{}^{\zeta}n_{i,j,k-\frac{1}{2}}\right)+F^{-}\left({}^{\zeta}w^{+}_{i,j,k-\frac{1}{2}},{}^{\zeta}n_{i,j,k-\frac{1}{2}}\right)+{}^{V}F_{i,j,k-\frac{1}{2}}\cdot{}^{\zeta}n_{i,j,k-\frac{1}{2}}\right] \end{array}\right] - S_{i,j,k} \quad (14)$$

$$\mu_T = C_\mu f_\mu(Re_T)\mu Re_T; \qquad C_\mu = 0.09$$

$$f_\mu(Re_T) = \exp\left[\frac{-3.4}{(1+0.02Re_T)^2}\right] \quad (9)$$

$$\kappa_T = \mu_T c_p/Pr_T; \qquad Pr_T = 0.9$$

$$\mu(\tilde{T}) = \mu_{273}\left[\frac{\tilde{T}}{273.15}\right]^{\frac{3}{2}}\frac{110.4+273.15}{110.4+\tilde{T}} \quad (10)$$

$$\kappa(\tilde{T}) = \kappa_{273}[\mu(\tilde{T})/\mu_{273}][1+0.00023(\tilde{T}-273.15)]$$

where $\mu_{273} = 17.11 \times 10^{-6}$ Pa s, and $\kappa_{273} = 0.0242$ Wm^{-1} K^{-1}.

Note that a source term is present in the mean-flow energy equation [Eq. (3)]. This term is necessary because the averaging operator $\overline{\rho h_t} = \overline{\rho h + (1/2)\rho u_i u_i} = \bar{\rho}\breve{h}_t + \bar{\rho}k$ introduces the turbulence kinetic energy $k = (1/2)\widetilde{u_i'' u_i''}$. Several authors include this term by introducing a modified pressure $p^* = \bar{p} + \frac{2}{3}\bar{\rho}k$ (Refs. 31 and 55), whereas others neglect it since it becomes important only in high-supersonic flows.[43,45] This new formulation introduces the correct fully coupled mean-flow energy equation, while avoiding the modified-pressure formulation.

Space-Discretization

These equations [Eqs. (1–5)] are discretized on a structured grid using a finite volume technique, with vertex storage. Defining the vector of unknowns w (not to be confused with the velocity component w)

$$w = [\bar{\rho}, \bar{\rho}\tilde{u}, \bar{\rho}\tilde{v}, \bar{\rho}\tilde{w}, \bar{\rho}\breve{h}_t - \bar{p}, \bar{\rho}k, \bar{\rho}\varepsilon^*]^T \in \mathbb{R}^7 \quad (11)$$

the Navier–Stokes [Eqs. (1–3)] and turbulence-transport equations [Eqs. (4) and (5)] can be written

$$\frac{\partial w}{\partial t} + \mathrm{div}[{}^{C}F(w) + {}^{V}F(w) + S(w)] = 0 \quad (12)$$

where the convective fluxes ${}^{C}F \in \mathbb{R}^7 \otimes \mathbb{R}^3$, the viscous fluxes ${}^{V}F \in \mathbb{R}^7 \otimes \mathbb{R}^3$, and the source terms $S(w) \in \mathbb{R}^7$ are easily identified from Eqs. (1–5). The divergence of convective fluxes is discretized using the flux-vector-splitting method of Van Leer[75] with third-order MUSCL interpolation[74] and Van Albada limiters.[87] The divergence of viscous fluxes is computed using the centered scheme described by Arnone.[88] The present implementation follows closely the work of Anderson et al.[76,77] Defining a staggered grid

$$x_{i\pm\frac{1}{2},j\pm\frac{1}{2},k\pm\frac{1}{2}} = \tfrac{1}{8}[x_{i,j,k} + x_{i\pm1,j,k} + x_{i\pm1,j\pm1,k} + x_{i,j\pm1,k} + x_{i,j,k\pm1} + x_{i\pm1,j,k\pm1} + x_{i\pm1,j\pm1,k\pm1} + x_{i,j\pm1,k\pm1}] \quad (13)$$

and noting (ξ, η, ζ) the grid directions (i, j, k), $({}^{\xi}\mathcal{S}_{i\pm(1/2),j,k}, {}^{\eta}\mathcal{S}_{i,j\pm(1/2),k}, {}^{\zeta}\mathcal{S}_{i,j,k\pm(1/2)})$ the cell-face areas of the staggered-grid cell around the point (i, j, k), and $({}^{\xi}n_{i\pm(1/2),j,k}, {}^{\eta}n_{i,j\pm(1/2),k}, {}^{\zeta}n_{i,j,k\pm(1/2)})$ the corresponding normals, the semidiscrete scheme can be written

where $\mathcal{V}_{i,j,k}$ is the control-volume computed as the sum of 6 pyramids.[89] The viscous fluxes at cell-faces are given by

$$\begin{aligned} {}^{V}F_{i\pm\frac{1}{2},j,k} &= \tfrac{1}{2}[{}^{V}F_{i,j,k} + {}^{V}F_{i\pm1,j,k}] \\ {}^{V}F_{i,j\pm\frac{1}{2},k} &= \tfrac{1}{2}[{}^{V}F_{i,j,k} + {}^{V}F_{i,j\pm1,k}] \\ {}^{V}F_{i,j,k\pm\frac{1}{2}} &= \tfrac{1}{2}[{}^{V}F_{i,j,k} + {}^{V}F_{i,j,k\pm1}] \end{aligned} \quad (15)$$

and the Van Leer fluxes are given by

$$F^{\pm} = \underbrace{\begin{bmatrix}0\\0\\0\\0\\0\\0\\0\end{bmatrix}}_{\pm M_n(w,n)<-1}$$

$$\underbrace{\pm\bar{\rho}a\frac{(M_n\pm1)^2}{4}\begin{bmatrix}1\\ n_x(a/\gamma)(-M_n\pm2)+\tilde{u}\\ n_y(a/\gamma)(-M_n\pm2)+\tilde{v}\\ n_z(a/\gamma)(-M_n\pm2)+\tilde{w}\\ \dfrac{-(\gamma-1)M_n^2\pm2(\gamma-1)M_n+2}{\gamma^2-1}a^2+\dfrac{\tilde{V}^2}{2}\\ k\\ \varepsilon^*\end{bmatrix}}_{|M_n(w,n)|\le1}$$

$$\underbrace{\begin{bmatrix}\bar{\rho}\tilde{V}_n\\ \bar{\rho}\tilde{V}_n\tilde{u}+\bar{p}n_x\\ \bar{\rho}\tilde{V}_n\tilde{v}+\bar{p}n_y\\ \bar{\rho}\tilde{V}_n\tilde{w}+\bar{p}n_z\\ \bar{\rho}\tilde{V}_n\breve{h}_t\\ \bar{\rho}\tilde{V}_nk\\ \bar{\rho}\tilde{V}_n\varepsilon^*\end{bmatrix}}_{\pm M_n(w,n)>1} \quad (16)$$

where $M_n(w, n) = \tilde{V}(w)\cdot n/a(w) = \tilde{V}_n/a$ and $a(w) = \sqrt{[\gamma R_g \tilde{T}(w)]}$. The MUSCL variables are given by

$$\begin{aligned} w^{\pm}_{i-\frac{1}{2},j,k} &= w^{\pm}\left(w_{i-\frac{3}{2}\pm\frac{1}{2},j,k}, w_{i-\frac{1}{2}\pm\frac{1}{2},j,k}, w_{i+\frac{1}{2}\pm\frac{1}{2},j,k}\right) \\ w^{\pm}_{i,j-\frac{1}{2},k} &= w^{\pm}\left(w_{i,j-\frac{3}{2}\pm\frac{1}{2},k}, w_{i,j-\frac{1}{2}\pm\frac{1}{2},k}, w_{i,j+\frac{1}{2}\pm\frac{1}{2},k}\right) \\ w^{\pm}_{i,j,k-\frac{1}{2}} &= w^{\pm}\left(w_{i,j,k-\frac{3}{2}\pm\frac{1}{2}}, w_{i,j,k,-\frac{1}{2}\pm\frac{1}{2}}, w_{i,j,k+\frac{1}{2}\pm\frac{1}{2}}\right) \end{aligned} \quad (17)$$

where the MUSCL interpolation $w^{\pm}$ and the Van Albada limiters s are

$$w^{\pm}(w_{-1}, w_0, w_{+1}) = w_0 \mp \{(s/4)[1 \mp (s/3)](w_{+1} - w_0) + (s/4)[1 \pm (s/3)](w_0 - w_{-1})\}$$

$$s(w_{-1}, w_0, w_{+1}) = \frac{2\mathrm{dif}(w_{+1}, w_0) \cdot \mathrm{dif}(w_0, w_{-1}) + 10^{-23}}{\mathrm{dif}(w_{+1}, w_0) \cdot \mathrm{dif}(w_{+1}, w_0) + \mathrm{dif}(w_0, w_{-1}) \cdot \mathrm{dif}(w_0, w_{-1}) + 10^{-23}} \tag{18}$$

where the 10^{-23} term is introduced to avoid division by 0 and

$$\mathrm{dif}(w_A, w_B) = \left[\frac{\bar\rho_A - \bar\rho_B}{\rho_{AB}}, \frac{\bar\rho_A \tilde u_A - \bar\rho_B \tilde u_B}{\rho_{AB} a_{AB}}, \frac{\bar\rho_A \tilde v_A - \bar\rho_B \tilde v_B}{\rho_{AB} a_{AB}}, \frac{\bar\rho_A \tilde w_A - \bar\rho_B \tilde w_B}{\rho_{AB} a_{AB}}, \frac{(\bar\rho_A \breve h_{t_A} - \bar p_A) - (\bar\rho_B \breve h_{t_B} - \bar p_B)}{\rho_{AB} a_{AB}^2}, 0, 0\right]^T \tag{19}$$

where $\rho_{AB} = \frac{1}{2}(\bar\rho_A + \bar\rho_B)$ and $\frac{1}{2}(a_A + a_B)$. The nondimensional differences are necessary because the present code is written directly in SI units, contrary to the usual nondimensional practice. Appropriate extrapolations are used at the boundaries of the computational domain.[90] Viscous stresses are computed using a centered second-order finite difference scheme.[88]

Time Integration

Denoting by $\mathcal{L}_{i,j,k}$ the discretized form of the space operator (divergence and source terms), the semi discrete equation at grid-point (i, j, k) gives

$$\frac{\mathrm{d}w_{i,j,k}}{\mathrm{d}t} + \mathcal{L}_{i,j,k} \cong 0 \quad \forall i, j, k \iff \frac{\mathrm{d}\mathfrak{w}}{\mathrm{d}t} + \mathfrak{L}(\mathfrak{w}) \cong 0 \tag{20}$$

where $\mathfrak{w} = [w_{1,1,1}, w_{1,1,2}, \ldots, w_{Ni,Nj,Nk}]^T \in \mathbb{R}^{7 \times Ni \times Nj \times Nk}$ and $\mathfrak{L} = [\mathcal{L}_{1,1,1}, \mathcal{L}_{1,1,2}, \ldots, \mathcal{L}_{Ni,Nj,Nk}]^T \in \mathbb{R}^{7 \times Ni \times Nj \times Nk}$ are the global vectors of the unknowns and space operators. The time discretization of the semidiscrete scheme uses a first-order implicit scheme, and can be written between instants n and $n+1$

$$\left(\mathfrak{I} + \Delta t \frac{\partial \mathfrak{L}}{\partial \mathfrak{w}}\right)({}^{n+1}\mathfrak{w} - {}^{n}\mathfrak{w}) \cong -\Delta t \mathfrak{L}({}^{n}\mathfrak{w}) \tag{21}$$

where $\mathfrak{I} \in \mathbb{R}^{(7 \times Ni \times Nj \times Nk) \times (7 \times Ni \times Nj \times Nk)}$ is the identity matrix and the Jacobian matrix $\partial \mathfrak{L}/\partial \mathfrak{w}$ is evaluated at time n. Any approximation of the system matrix will retain formal first-order time-accuracy, which is sufficient for steady computations. The resulting linear system is solved after approximate factorization of the Jacobian matrix of convective and viscous fluxes and source terms. The bandwidth of the spacewise systems is reduced using a spatially first-order accurate approximation for the implicit term. Viscous terms are treated using a spectral radius approximation.

$$\begin{aligned}
&\Delta t_{i,j,k}\, {}^{\xi}\boldsymbol{A}_{i+1,j,k}\, {}^{\xi}\Delta w_{i+1,j,k} + \left(\mathbf{1} + \Delta t_{i,j,k}\, {}^{\xi}\boldsymbol{A}_{i,j,k}\right) {}^{\xi}\Delta w_{i,j,k} \\
&\quad + \Delta t_{i,j,k}\, {}^{\xi}\boldsymbol{A}_{i-1,j,k}\, {}^{\xi}\Delta w_{i-1,j,k} = -\Delta t_{i,j,k}\, {}^{n}\mathcal{L}_{i,j,k} \\
&\Delta t_{i,j,k}\, {}^{\eta}\boldsymbol{A}_{i,j+1,k}\, {}^{\eta}\Delta w_{i,j+1,k} + \left(\mathbf{1} + \Delta t_{i,j,k}\, {}^{\eta}\boldsymbol{A}_{i,j,k}\right) {}^{\eta}\Delta w_{i,j,k} \\
&\quad + \Delta t_{i,j,k}\, {}^{\eta}\boldsymbol{A}_{i,j-1,k}\, {}^{\eta}\Delta w_{i,j-1,k} = {}^{\xi}\Delta w_{i,j,k} \\
&\Delta t_{i,j,k}\, {}^{\zeta}\boldsymbol{A}_{i,j,k+1}\, {}^{\zeta}\Delta w_{i,j,k+1} + \left(\mathbf{1} + \Delta t_{i,j,k}\, {}^{\zeta}\boldsymbol{A}_{i,j,k}\right) {}^{\zeta}\Delta w_{i,j,k} \\
&\quad + \Delta t_{i,j,k}\, {}^{\zeta}\boldsymbol{A}_{i,j,k-1}\, {}^{\zeta}\Delta w_{i,j,k-1} = {}^{\eta}\Delta w_{i,j,k} \\
&\left(\mathbf{1} + \Delta t_{i,j,k} \frac{\partial S}{\partial w}\left({}^{n}w_{i,j,k}\right)\right)\Delta w_{i,j,k} = {}^{\zeta}\Delta w_{i,j,k}
\end{aligned} \tag{22}$$

The three successive spacewise linear systems are solved using banded lower–upper (LU) factorization.[91] The corresponding bandwidth is $(1 + 2 \times 13)$. The implicit phase for the source-terms involves only the local inversion of a 2×2 matrix. The 7×7 real matrices ${}^{\xi,\eta,\zeta}\boldsymbol{A}_{i\pm1,j\pm1,k\pm1}$, ${}^{\xi,\eta,\zeta}\boldsymbol{A}_{i,j,k}$, $\partial S/\partial w$, are given in Vallet.[92]

Local Time Step

The local time step is based on a combined convective (Courant) and viscous (von Neumann) criterion[46]:

$$\Delta t_{i,j,k} \le \mathrm{CFL} \min\left\{\frac{\ell_g}{\tilde V + a\sqrt{1 + (5/3)(\gamma - 1)(k/a^2)}}, \frac{\ell_g^2}{2\nu_{\mathrm{eq}}}\right\} \forall i, j, k$$

$$\nu_{\mathrm{eq}} = \max\left\{\tfrac{4}{3}(\nu + \nu_T), [(\gamma - 1)/\rho R_g](\kappa + \kappa_T)\right\} \tag{23}$$

where ℓ_g is the grid cell size, $\tilde V$ the flow velocity, a the sound velocity, and ν_{eq} the equivalent diffusivity, computed by MacCormack.[59] Note that the turbulence Mach number[18] $M_T = \sqrt{(2ka^{-2})}$ appears in the convective stability time step, as has been demonstrated by many authors.[27,31,46] The particular form used here was given recently by Raulot[93] and is based on a one-dimensional stability analysis. For steady computations, a CFL = 50 is used with local time stepping.

Boundary Conditions

To achieve the high time steps used and the associated rapid convergence rate, it is indispensible to apply boundary conditions both implicitly and explicitly. The following boundary conditions were implemented.

Inflow reservoir condition:

$$\frac{\partial \breve s}{\partial t} = 0; \quad \frac{\partial \breve h_t}{\partial t} = 0; \quad \frac{\partial[\tilde V - (\tilde V \cdot n)n]}{\partial t} = 0; \quad \frac{\partial k}{\partial t} = 0; \quad \frac{\partial \varepsilon^*}{\partial t} = 0 \tag{24}$$

Adiabatic wall condition:

$$\tilde V = 0; \quad \frac{\partial \bar p}{\partial n} = 0; \quad \frac{\partial \tilde T}{\partial n} = 0; \quad k = 0; \quad \varepsilon^* = 0 \tag{25}$$

Outflow pressure condition:

$$\frac{\partial \bar p}{\partial t} = 0; \quad \frac{\partial \bar\rho}{\partial n} = 0; \quad \frac{\partial \tilde V}{\partial n} = 0; \quad \frac{\partial k}{\partial n} = 0; \quad \frac{\partial \varepsilon^*}{\partial n} = 0 \tag{26}$$

Plane-of-symmetry condition:

$$\frac{\partial w}{\partial n} = 0; \quad \tilde V \cdot n = 0 \tag{27}$$

where $\breve s = s(\bar p, \tilde T)$ is the entropy and n the unit normal to the boundary. The inflow boundary condition is implemented using the theory of finite waves[94] and is treated implicitly following the corrections method of Chakravarthy,[95] to account for the outgoing pressure wave.

Initialization

The authors believe that for practical purposes a Navier–Stokes solver must be able to start from a simple initialization of the flowfield. For stability it is best to fit analytic flat-plate profiles at solid boundaries. These profiles are fitted to a simple inviscid flowfield obtained by linearly interpolating pressure between inflow and outflow, and assuming isentropic adiabatic evolution. The mean flow and turbulence profiles are obtained analytically in a manner similar to that of Gerolymos.[43] In the case of solid corners, the two-dimensional profiles are extended to three dimensional using a simple blending rule, based on the distance from the walls. The details for the initialization procedure are given in Vallet.[92]

k–ε Positivity and Boundedness

To ensure the stability of the method, it is necessary to introduce limiters for k and ε, which may otherwise diverge towards nonphysical values. The following very simple and particularly efficient limiters were used:

$$\text{if}\left\{k < 0 \vee \varepsilon^* < 0 \vee \ell_T \doteq \left(k^{\frac{3}{2}}/\varepsilon^*\right) > \ell_{T_{\max}}\right\} : \{k \leftarrow 0 \wedge \varepsilon^* \leftarrow 0\} \tag{28}$$

where $\ell_{T_{\max}}$ is a maximum admissible length scale (a characteristic order-of-magnitude length of the configuration). Divisions by 0 are avoided throughout the code by adding 10^{-23} to the denominator [e.g., when $k = 0$ and $\varepsilon^* = 0$, $k^2/\varepsilon^* \cong k^2/(\varepsilon^* + 10^{-23}) = 0$ and $\varepsilon^{*2}/k \cong \varepsilon^{*2}/(k + 10^{-23}) = 0$]. Also, following Turner and Jennions[51] and Jennions and Turner,[52] the production of turbulence kinetic energy was limited to twice the dissipation:

$$P_k \leftarrow \min\{P_k, 2\rho\varepsilon^*\} \tag{29}$$

These simple positivity and boundedness fixes stabilize the computations in all of the cases studied in this paper and also in more complex configurations such as wings and turbomachinery cascades.[96] They are less stringent and more effective than the limiters used previously by Gerolymos,[43] the main advantage coming from fixing k and ε^* to 0 and not appropriating small values as is usually done.[27,43,45,46]

Results

Configurations Studied

The numerical method described in this paper was applied to several transonic channel configurations (Table 2), for which experimental measurements were available.[55,97,98] The first three configurations are nominally two dimensional, although as will be shown in the following, they are contaminated by three-dimensional effects, because of the shock-wave/boundary-layer interaction at the channel-corners. The last configuration is fully three dimensional (geometrically). Because of paper length limitations, only a few of the results detailed in Vallet[92] are presented.

Two-Dimensional Results for Délery Nozzles

Initial computations were run in pseudo-two-dimensional mode using the three-dimensional code. For these computations five equidistant mesh planes were used in the lateral direction (z wise) with symmetry conditions on the sidewalls. The computational grid is generated algebraically. It consists of planes perpendicular to the x axis, equidistant between the inflow and outflow stations. In the y direction the mesh is stretched geometrically. The same y_w^+ is used on both the upper and lower walls, with the same geometric-progression ratio r_y, so that (with the constraint N_j odd) the upper and lower wall progressions match at half-distance. The two-dimensional results[92] are typical for these configurations and agree with results obtained with different numerical methods.[43,49,50]

Influence of n_w^+ and CFL Number on Results

To demonstrate that results are independent of time step, computations for Délery B nozzle, using the fine 177 × 193 grid with $y_w^+ = 0.45$ (Table 3), were run for CFL numbers 40, 50, 60, and 80. Comparison of the isentropic wall Mach-number distributions shows[92] that there is practically no dependence on time step, whereas consideration of the number of iterations to convergence (Table 4) indicates that CFL $\sim$ 50 is nearly optimal.

The importance of grid refinement on results has been discussed recently by Roache,[99] who introduced the important concept of grid-convergence index. This concept is unfortunately not applicable as such to the grids used in this study because the grids are dependent on two parameters, the number of points (N_i, N_j, N_k) and the size of the first cell nearest the wall n_w^+. Practical experience of virtually all users of near-wall turbulence closures (e.g., Table 1) suggests that n_w^+ is the most important parameter concerning grid quality. In other words the grids necessary for near-wall turbulence closures depend both on linear refinement (for the away from the wall regions) and on the nonlinear one associated with the viscous sublayer resolution. This nonlinear refinement is characterized by the stretching used (exponential, geometric) and n_w^+. To illustrate this point pseudo-two-dimensional computations were run, for the Délery A nozzle using four different grids with the same x-wise resolution ($N_i = 129$), which differ in the y direction (Table 3). The first two grids have both $N_j = 129$, but one ($N_j = 129$, $y_w^+ = 0.41$) is more stretched than the other ($N_j = 129$, $y_w^+ = 1.09$), which is evidently finer away from the wall (Fig. 1). Then two other grids ($N_j = 115$, $y_w^+ = 1.00$) and ($N_j = 111$, $y_w^+ = 1.50$) were used that have the same mesh size at the nozzle axis as the ($N_j = 129$, $y_w^+ = 0.41$) grid but are less stretched. Such grids are often tempting to industrial users, as they permit less expensive computations, not only because they have less points (an effect that is more pronounced in three dimensions) but also because the coarser near-wall mesh means higher time steps and associated faster convergence (less iterations). Consideration of results (Fig. 1) shows clearly that the single most important parameter is n_w^+. Grids ($N_j = 129$, $y_w^+ = 1.09$) and ($N_j = 115$, $y_w^+ = 1.00$) give practically identical results, although the second is coarser at the axis. In general, lower n_w^+ corresponds to lower computed viscous losses

Table 2 Configurations studied

Case	Description	$L_x \times L_y \times L_z$, mm	M_{shock}	Chord (χ, mm)	Re_χ	Computation
Délery A[97]	Two symmetric bumps	500 × 100 × 120.0	1.30	200	2.0×10^6	Two dimensional
Délery B[97]	Two symmetric bumps	550 × 100 × 120.0	1.45	269	2.5×10^6	Two and three dimensional
Délery C[97]	Bump on lower wall	500 × 100 × 120.0	1.36	286	2.8×10^6	Two dimensional
Délery three dimensional[55,98]	Three-dimensional bump on lower wall	800 × 100 × 121.3	1.83	245–370	2.2–3.3×10^6	Three dimensional

Table 3 Computational grids summary

Case	$N_i(N_x)$	$N_j(N_y)$	$N_k(N_z)$	y_w^+	z_w^+	r_y	r_z	Computation
Délery A	129	129	5	0.41	——	1.1500	——	Pseudo-two dimensional
	129	129	5	1.09	——	1.1300	——	Pseudo-two dimensional
	129	115	5	1.00	——	1.1550	——	Pseudo-two dimensional
	129	111	5	1.50	——	1.1525	——	Pseudo-two dimensional
	177	193	5	0.41	——	1.0920	——	Pseudo-two dimensional
Délery B	129	129	5	0.38	——	1.1500	——	Pseudo-two dimensional
	177	193	5	0.45	——	1.0900	——	Pseudo-two dimensional
	161	65	65	0.48	0.46	1.1450	1.1500	Three dimensional
	161	65	97	0.48	0.46	1.1450	1.0920	Three dimensional
Délery C	129	129	5	0.40	——	1.1500	——	Pseudo-two dimensional
	177	193	5	0.50	——	1.0900	——	Pseudo-two dimensional
Délery three dimensional	121	49	49	1.50	1.50	1.5100	1.4440	Three dimensional
	201	91	101	0.75	0.75	1.2155	1.1935	Three dimensional

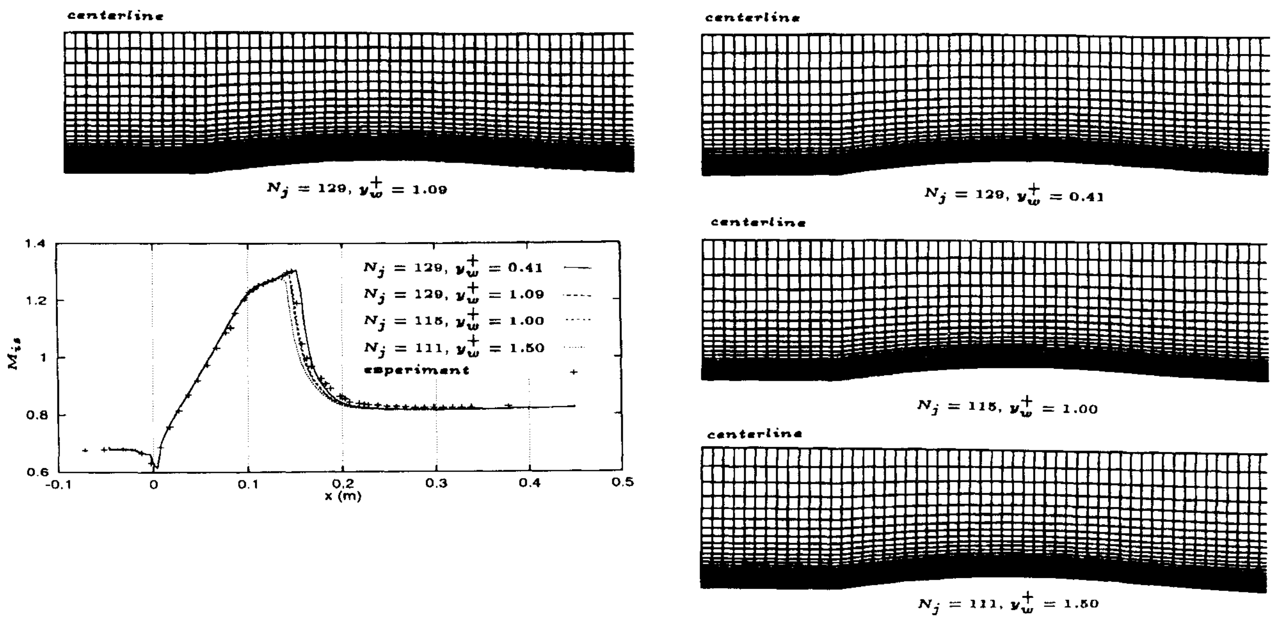

Fig. 1 Influence of n_w^+ on results for Délery A nozzle.

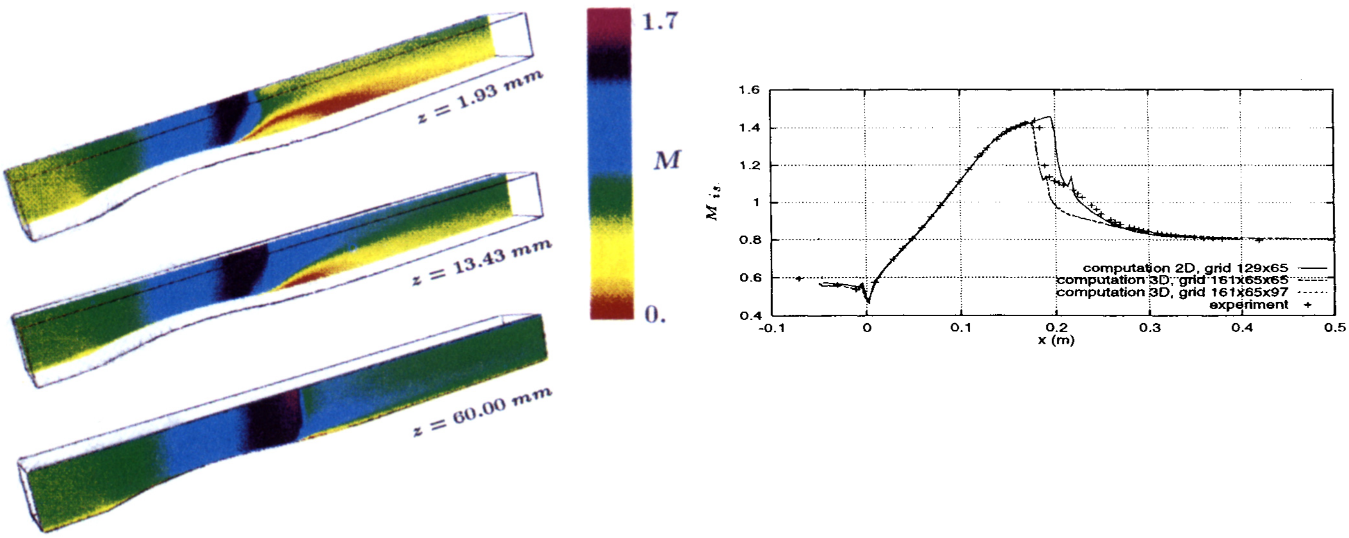

Fig. 2 Comparison of two- and three-dimensional computations with experiment for Délery B nozzle.

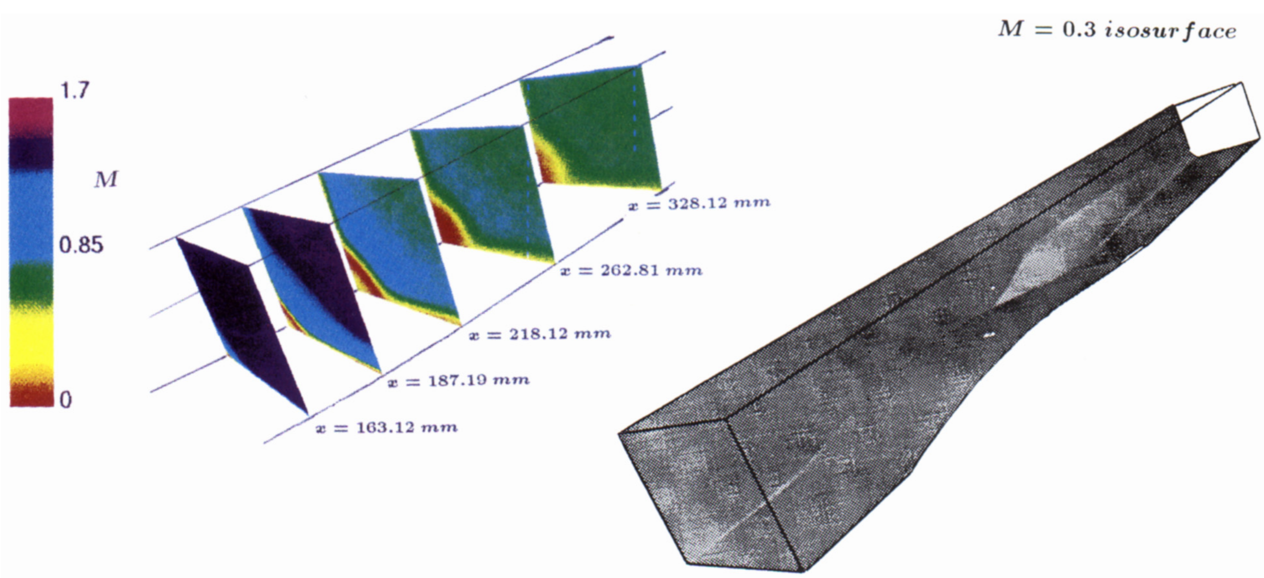

Fig. 3 Three-dimensional separation at the sidewall corner for Délery B nozzle.

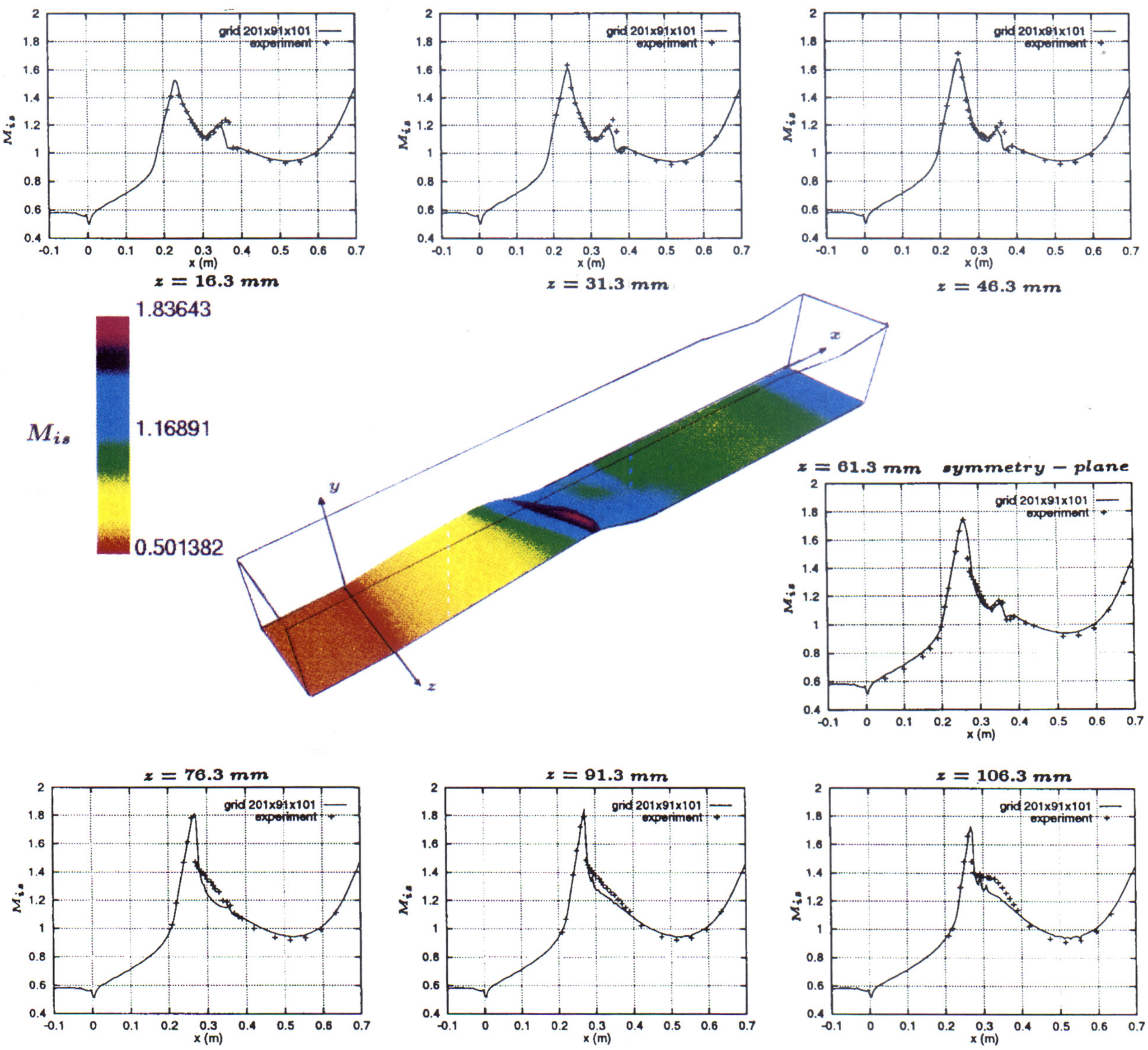

Fig. 4 M_{is_w} distributions for Délery three-dimensional nozzle.

Table 4 Influence of CFL number on convergence

CFL	Iterations to convergence
40	1600
50	1400
60	2000
80	2000

and as a consequence a more downstream position of the shock wave.

Three-Dimensional Effects for Délery B Nozzle

To assess the importance of three-dimensional effects for Délery B nozzle three-dimensional computations were run. Only $\frac{1}{4}$ of the nozzle was discretized, and symmetry conditions were imposed at the y- and z-wise symmetry planes. The grid was stretched both y wise and z wise as described in the two-dimensional computations section. Computations were run with two grids (Table 3) for which $y_w^+ \cong z_w^+ \cong 0.5$. For both grids the mesh at the y-symmetry plane is identical with the one used for the pseudo-two-dimensional computations (notice that now only one-half of the nozzle height is discretized so that 65 points correspond to $\frac{1}{2}$ of 129, and that the outflow boundary was placed farther downstream). Both grids yield identical results (Fig. 2), showing that no further z-wise refinement is necessary.

There is a substantial difference in isentropic wall Mach-number distribution between the three-dimensional and the pseudo-two-dimensional computations (Fig. 2), suggesting that three-dimensional effects are substantial. This is clearly seen in the isoplots of Mach number at three different positions away from the sidewall (Fig. 2) that suggest the presence of important boundary-layer separation at the corner between the lower wall and the sidewall, because of the three-dimensional shock-wave/boundary-layer interaction. This interaction is better understood considering

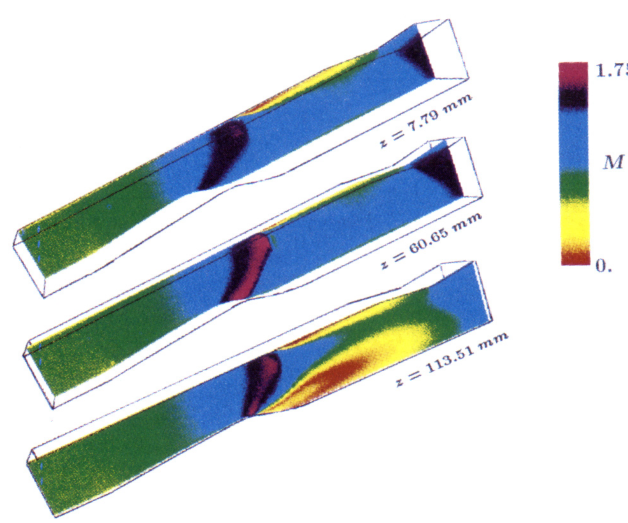

Fig. 5 Iso-Machs for Délery three-dimensional nozzle.

Table 5 Computing time requirements for three-diamensional computations

Case	Grid ($N_i \times N_j \times N_k$)	Mpoints[a]	Mwords	y_w^+	z_w^+	Iterations	CPU, h[b]
Délery B	161 × 65 × 65	0.65	53	0.48	0.46	900	14
	161 × 65 × 97	0.97	82	0.48	0.46	1000	21
Délery three dimensional	121 × 49 × 49	0.28	25	1.50	1.50	300	3
	201 × 91 × 101	1.76	141	0.75	0.75	900	31

[a] One Mpoints = 1024^2. [b]Cray C-98.

the iso-Machs at various x-wise planes, in the neighborhood of the interaction (Fig. 3) illustrating the detachment and reattachment of the boundary layer. The surface on which $\breve{M} = 0.3$ (Fig. 3) shows clearly the displacement effect on the sidewall. This three-dimensional effect induces a shock wave that is much farther upstream than the one computed on the assumption that the flow is two dimensional. The comparison of the three-dimensional computation with experiment is fair but far from satisfactory. Although the shock wave is now placed at almost the right position (Fig. 2), the subsequent boundary-layer detachment is grossly underestimated, because of the inadequacy of the k–ε model.

Délery Three-Dimensional Nozzle

This configuration consists of a swept three-dimensional bump on the lower wall. The upper wall is slightly sloped downward, and the two sidewalls are parallel planes. As in all preceding cases the experimental setup includes an adjustable second throat, which is used to generate and adjust the shock wave.[97,98] Contrary to the usual computational practice of imposing a constant back pressure (which was also used in the preceding sections) it was preferred to include the second throat in the computations. The flow is accelerated to a supersonic exit, and the shock-wave position is adjusted by the second throat area. Initial tests using a very coarse $\sim 0.28M$ points grid (Table 3) were used to determine the throat height.

Results using a $\sim 1.76M$ points grid (Table 3) with $y_w^+ = z_w^+ = 0.75$ show quite satisfactory agreement with the measured isentropic wall Mach-number distributions on the lower wall (Fig. 4). The agreement is remarkable at the symmetry plane ($z = 61.3$ mm) where the λ shock wave is accurately predicted. The agreement is fair but less satisfactory near the sidewalls. Toward the far wall (shorter bump) there appears, in both the experiment and the computations, the λ shock-wave structure, but although the position of the first shock wave is well predicted, the computations underestimate the strength of the second shock wave. Toward the near wall (longer bump) the shock wave is stronger and the computations underestimate the detachment of the boundary layer after the interaction and fail to predict the pressure-plateau at the near-wall corner.

The flow structure is shown in the iso-Machs plots (Fig. 5). There is a large recirculation zone at the lower wall near the corner because of the strong shock wave ($M_{is_w} \sim 1.8$), whereas the flow remains attached at the far corner. The shock wave on the upper wall is quite strong ($M_{is_w} \sim 1.65$), and there is a noticeable boundary-layer separation that spans the entire channel width.

Computing Time Requirements

The code runs on a Cray C-98 computer. Its vectorization is adequate but not outstanding (~250 Mflops), and computing-time requirements (Table 5) can still be substantially reduced. The computing time necessary for the pseudo-two-dimensional computations is not presented because it cannot be compared with two-dimensional methods (five transverse planes are used). Note that a deliberate choice was made to minimize memory requirements, even at a small sacrifice of computational rapidity (the linear systems are solved on a plane-by-plane basis and not on a global one, thus diminishing vector performance).

Conclusions

In the present work an efficient and robust computational method for the numerical integration of the compressible Navier–Stokes equations with near-wall k–ε closure was developed. The method has optimal convergence (for all of the cases studied) at CFL = 50 and runs from a simple automatic initialization of the flowfield. The time steps obtained are quite large compared with the state of the art of time-marching schemes using k–ε closure for transonic flows. The code is written in SI units.

The results obtained are typical of the near-wall k–ε closure. Nonetheless the three-dimensional computations of the Délery B test case highlight a particularly important and usually neglected feature of nominally two-dimensional transonic shock-wave/boundary-layer experiments, i.e., that they are really three dimensional and should be used for code validation as such. Although, because of the inaccuracy of the k–ε closure, the agreement of the three-dimensional computations with experiment is not quite satisfactory, the difference between two- and three-dimensional results, obtained by the same code on the same grid, underlines the importance of three-dimensional effects in this case and raises the question of validity of two-dimensional computations that would accurately reproduce this flow. This does not negate the importance of such experiments: it is simply necessary to compute the full three-dimensional configuration.

The satisfactory results for the Délery three-dimensional case are mainly because of the simulation of the second throat. This is very important because there exists no plane before the throat where static pressure is nearly homogeneous.

A grid refinement study has confirmed that n_w^+ is the single most important parameter for accuracy (for transonic flows it is necessary that $n_w^+ \leq 0.75$). In general, lower n_w^+ corresponds to lower computed viscous losses and, as a consequence, a more downstream position of the shock wave. This study has shown that the concept of grid convergence index is not applicable in the case of grids dependent on two parameters, the number of points and the size of the first cell nearest the wall n_w^+.

The authors are working on many improvements. In order of importance the improvements are improvement of the turbulence model using full Reynolds-stress near-wall closures; the use of accurate Jacobians for the viscous fluxes and eventually of nonfactored implicit schemes, although these would only become competitive for optimal CFL > 500 and can only be implemented in large-memory systems (for the three-dimensional grids used in this study); and the improvement of the space discretization using advanced upwind techniques.

Acknowledgments

The computations presented were run at the Institut pour le Développement des Ressources en Informatique Scientifique, where computer resources were made available by the Comité Scientifique. The authors wish to thank J. M. Délery for providing the experimental data and discussing the results. The authors are listed alphabetically.

References

[1]Patel, V. G., Rodi, W., and Scheuerer, G., "Turbulence Models for Near-Wall and Low-Reynolds-Number Flows: A Review," *AIAA Journal*, Vol. 23, 1985, pp. 1308–1319.

[2]Lakshminarayana, B., "Turbulence Modeling for Complex Shear Flows," *AIAA Journal*, Vol. 24, 1986, pp. 1900–1917.

[3]Jones, W. P., and Launder, B. E., "The Prediction of Laminarization with a 2-Equation Model of Turbulence," *International Journal of Heat and Mass Transfer*, Vol. 15, 1972, pp. 301–314.

[4]Jones, W. P., and Launder, B. E., "The Calculation of Low-Reynolds-Number Phenomena with a 2-Equation Model of Turbulence," *International Journal of Heat and Mass Transfer*, Vol. 16, 1973, pp. 1119–1130.

[5]Launder, B. E., and Sharma, B. I., "Application of the Energy Dissipation Model of Turbulence to the Calculation of Flows Near a Spinning Disk," *Letters in Heat and Mass Transfer*, Vol. 1, 1974, pp. 131–138.

[6]Chien, K. Y., "Predictions of Channel and Boundary-Layer Flows with a Low-Reynolds Number Turbulence Model," *AIAA Journal*, Vol. 20, 1982, pp. 33–38.

[7]Coakley, T. J., "Turbulence Modeling Methods for Compressible Navier–Stokes Equations," AIAA Paper 83-1693, 1983.

[8]Wilcox, D. C., "Reassessment of the Scale-Determining Equation for Advanced Turbulence Models," *AIAA Journal*, Vol. 26, 1988, pp. 1299–1310.

[9]Speziale, C. G., "On Nonlinear k–ℓ and k–ε Models of Turbulence," *Journal of Fluid Mechanics*, Vol. 178, 1987, pp. 459–475.

[10]Thangam, S., and Speziale, C. G., "Turbulent Flow Past a Backward-Facing Step: A Critical Evaluation of 2-Equation Models," *AIAA Journal*, Vol. 30, 1992, pp. 1314–1320.

[11]Lien, F. S., and Leschziner, M. A., "Assessment of Turbulence-Transport Models Including Nonlinear RNG Eddy-Viscosity Formulation and 2-Moment Closure for Flow over a Backward-Facing Step," *Computers and Fluids*, Vol. 23, 1994, pp. 983–1004.

[12]Launder, B. E., and Shima, N., "2-Moment Closure for the Near-Wall Sublayer: Development and Application," *AIAA Journal*, Vol. 27, 1989, pp. 1319–1325.

[13]So, R. M. C., Lai, Y. G., and Hwang, B. C., "Near-Wall Turbulence Closure for Curved Flows," *AIAA Journal*, Vol. 29, 1991, pp. 1202–1213.

[14]So, R. M. C., Lai, Y. G., Zhang, H. S., and Hwang, B. C., "Two-Order Near-Wall Turbulence Closures: A Review," *AIAA Journal*, Vol. 29, 1991, pp. 1819–1835.

[15]So, R. M. C., Zhang, H. S., and Speziale, C. G., "Near-Wall Modeling of the Dissipation-Rate Equation," *AIAA Journal*, Vol. 29, 1991, pp. 2069–2076.

[16]Sotiropoulos, F., and Patel, V. C., "Prediction of Turbulent Flow Through a Transition Duct Using a 2-Moment Closure," *AIAA Journal*, Vol. 32, 1994, pp. 2194–2204.

[17]Zeman, O., "Dilatational Dissipation: The Concept and Application in Modeling Compressible Mixing-Layers," *Physics of Fluids A*, Vol. 2, 1990, pp. 178–188.

[18]Sarkar, S., and Lakshmanan, B., "Application of a Reynolds Stress Turbulence Model to the Compressible Shear Layer," *AIAA Journal*, Vol. 29, 1991, pp. 743–749.

[19]Wilcox, D. C., "Dilatation–Dissipation Corrections for Advanced Turbulence Models," *AIAA Journal*, Vol. 30, 1992, pp. 2639–2646.

[20]Sommer, T. P., So, R. M. C., and Zhang, H. S., "Near-Wall Variable-Prandtl-Number Turbulence Model for Compressible Flows," *AIAA Journal*, Vol. 31, 1993, pp. 27–35.

[21]Zhang, H. S., So, R. M. C., Speziale, C. G., and Lai, Y. G., "Near-Wall Two-Equation Model for Compressible Turbulent Flows," *AIAA Journal*, Vol. 31, 1993, pp. 196–199.

[22]Launder, B. E., "Numerical Computation of Convective Heat Transfer in Complex Turbulent Flows: Time to Abandon Wall-Functions?," *International Journal of Heat and Mass Transfer*, Vol. 27, 1984, pp. 1485–1491.

[23]Launder, B. E., "2-Moment Closure and Its Use in Modelling Turbulent Industrial Flows," *International Journal for Numerical Methods in Fluids*, Vol. 9, 1989, pp. 963–985.

[24]Leschziner, M. A., "Computation of Aerodynamic Flows with Turbulence-Transport Models Based on 2-Moment Closure," *Computers and Fluids*, Vol. 24, 1995, pp. 377–392.

[25]Courant, R., Friedrichs, K., and Lewy, H., "Über die partiellen Differenzgleichungen der mathematischen Physik," *Mathematische Annalen*, Vol. 100, 1928, pp. 32–74.

[26]Launder, B. E., and Spalding, D. B., "The Numerical Computation of Turbulent Flows," *Computational Methods in Applied Mechanics and Engineering*, Vol. 3, 1974, pp. 269–289.

[27]Coakley, T. J., and Viegas, J. R., "Turbulence Modeling of Shock-Separated Boundary-Layer Flows," Symposium on Turbulent Shear Flows, Pennsylvania State Univ., College Park, PA, 1977.

[28]Viegas, J. R., and Coakley, T. J., "Numerical Investigation of Turbulence Models for Shock Boundary-Layer Flows," *AIAA Journal*, Vol. 16, 1978, pp. 293, 294.

[29]Viegas, J. R., and Horstman, C. C., "Comparison of Multiequation Turbulence Models for Several Shock Boundary-Layer Interaction Flows," *AIAA Journal*, Vol. 17, 1979, pp. 811–820; also AIAA Paper 78-1165.

[30]Coakley, T. J., "Implicit Upwind Methods for the Compressible Navier–Stokes Equations," *AIAA Journal*, Vol. 23, 1985, pp. 374–380; also NASA TM 85899.

[31]Vandromme, D., and Ha Minh, H., "About the Coupling of Turbulence Closure Models with Averaged Navier–Stokes Equations," *Journal of Computational Physics*, Vol. 65, 1986, pp. 386–409.

[32]Horstman, C. C., "Computation of Sharp-Fin-Induced Shock-Wave/Turbulent-Boundary-Layer Interactions," *AIAA Journal*, Vol. 24, 1986, pp. 1433–1440.

[33]Knight, D. D., Horstman, C. C., Shapey, B., and Bogdonoff, S., "Structure of Supersonic Turbulent Flow Past a Sharp Fin," *AIAA Journal*, Vol. 25, 1987, pp. 1331–1337.

[34]Horstman, C. C., "Prediction of Secondary Separation in Shock-Wave/Boundary-Layer Interactions," *Computers and Fluids*, Vol. 17, 1989, pp. 611–614.

[35]Settles, G. S., Horstman, C. C., and McKenzie, T. M., "Experimental and Computational Study of a Swept Compression Corner Interaction Flowfield," *AIAA Journal*, Vol. 24, 1986, pp. 744–752.

[36]Knight, D. D., Horstman, C. C., and Bogdonof, S., "Structure of Supersonic Turbulent Flow Past a Swept Compression Corner," *AIAA Journal*, Vol. 30, 1992, pp. 890–896.

[37]Narayanswami, N., Knight, D. D., Bogdonof, S., and Horstman, C. C., "Interaction Between Crossing Oblique Shocks and a Turbulent Boundary-Layer," *AIAA Journal*, Vol. 30, 1992, pp. 1945–1952.

[38]Knight, D. D., Badekas, D., Horstman, C. C., and Settles, G. S., "Quasiconical Flowfield Structure of the Three-Dimensional Single Fin Interaction," *AIAA Journal*, Vol. 30, 1992, pp. 2809–2816.

[39]Sahu, J., and Danberg, J. E., "Navier–Stokes Computations of Transonic Flows with a Two-Equation Turbulence Model," *AIAA Journal*, Vol. 24, 1986, pp. 1744–1751.

[40]Kwon, O. K., "Navier–Stokes Solution for Steady 2-D Transonic Cascade Flows," *Journal of Turbomachinery*, Vol. 110, 1988, pp. 339–346.

[41]Knight, C. J., and Choi, D., "Development of a Viscous Cascade Code Based on Scalar Implicit Factorization," *AIAA Journal*, Vol. 27, 1989, pp. 581–590.

[42]Yokota, J. W., "Diagonally Inverted Lower-Upper Factored Implicit Multigrid Scheme for the 3-D Navier–Stokes Equations," *AIAA Journal*, Vol. 28, 1990, pp. 1642–1649.

[43]Gerolymos, G. A., "Implicit Multiple-Grid Computation of the Compressible Navier–Stokes Equations Using k–ε Turbulence Closure," *AIAA Journal*, Vol. 28, 1990, pp. 1707–1717.

[44]Hah, C., and Selva, R. J., "Navier–Stokes Analysis of Flow and Heat Transfer Inside High-Pressure-Ratio Transonic Turbine Blade-Rows," *Journal of Propulsion and Power*, Vol. 7, 1991, pp. 990–996.

[45]Kunz, R. F., and Lakshminarayana, B., "Explicit Navier–Stokes Computation of Cascade Flows Using the k–ε Turbulence Model," *AIAA Journal*, Vol. 30, 1992, pp. 13–22.

[46]Kunz, R. F., and Lakshminarayana, B., "Stability of Explicit Navier–Stokes Procedures Using k–ε and k–ε/Algebraic Reynolds Stress Turbulence Models," *Journal of Computational Physics*, Vol. 103, 1992, pp. 141–159.

[47]Rizzetta, D. P., "Numerical Simulation of Slot-Injection into a Turbulent Supersonic Stream," *AIAA Journal*, Vol. 30, 1992, pp. 2434–2439.

[48]Ameri, A. A., Sockol, P. M., and Gorla, R. S. R., "Navier–Stokes Analysis of Turbomachinery Blade External Heat Transfer," *Journal of Propulsion and Power*, Vol. 8, 1992, pp. 374–381.

[49]Leschziner, M. A., Dimitriadis, K. P., and Page, G., "Computational Modelling of Shock-Wave/Boundary-Layer Interaction with a Cell-Vertex Scheme and Transport Models of Turbulence," *Aeronautical Journal*, Vol. 97, 1993, pp. 43–61.

[50]Lien, F. S., and Leschziner, M. A., "A Pressure-Velocity Solution Strategy for Compressible Flow and Its Application to Shock/Boundary-Layer Interaction Using Second-Moment Closure," *Journal of Fluids Engineering*, Vol. 115, 1993, pp. 717–725.

[51]Turner, M. G., and Jennions, I. K., "An Investigation of Turbulence Modeling in Transonic Fans Including a Novel Implementation of an Implicit k–ε Turbulence Model," *Journal of Turbomachinery*, Vol. 115, 1993, pp. 249–260.

[52]Jennions, I. K., and Turner, M. G., "3-D Navier–Stokes Computations of Transonic Fan Flow Using an Explicit Flow Solver and an Implicit k–ε Turbulence Model," *Journal of Turbomachinery*, Vol. 115, 1993, pp. 261–272.

[53]Rizzetta, D. P., "Numerical Simulation of Turbulent Cylinder Juncture Flowfields," *AIAA Journal*, Vol. 32, No. 6, 1994, pp. 1113–1119.

[54]Liu, F., and Zheng, X., "Staggered Finite-Volume Scheme for Solving Cascade Flow with a k–ω Turbulence Model," *AIAA Journal*, Vol. 32, No. 9, 1994, pp. 1589–1597.

[55]Cahen, J., Couailler, V., Délery, J. M., and Pot, T., "Validation of Code Using Turbulence Model Applied to Three-Dimensional Transonic Channel," *AIAA Journal*, Vol. 33, No. 4, 1995, pp. 671–679.

[56]Zheng, X., and Liu, F., "Staggered Upwind Method for Solving Navier–Stokes and k–ω Turbulence Model Equations," *AIAA Journal*, Vol. 33, No. 6, 1995, pp. 991–998.

[57]Kwon, O. J., and Hah, C., "Simulation of Three-Dimensional Turbulent Flows on Unstructured Meshes," *AIAA Journal*, Vol. 33, No. 6, 1995, pp. 1081–1089.

[58]Lin, H., Yang, D. Y., and Chieng, C. C., "Variants of Biconjugate-Gradient Method for Compressible Navier–Stokes Solver," *AIAA Journal*, Vol. 33, No. 7, 1995, pp. 1177–1184.

[59]MacCormack, R. W., "A Numerical Method for Solving the Equations of Compressible Viscous Flow," *AIAA Journal*, Vol. 20, 1982, pp. 1275–1281.

[60]Beam, R., and Warming, R. F., "An Implicit Factored Scheme for the Compressible Navier–Stokes Equations," *AIAA Journal*, Vol. 16, 1978, pp. 393–402.

[61]Gordon, P., "Nonsymmetric Difference Equations," *SIAM Journal*, Vol. 1, 1965, pp. 667–673.

[62]Scala, S. M., and Gordon, P., "Solution of the Time-Dependent Navier–Stokes Equations for Flow Around a Circular Cylinder," *AIAA Journal*, Vol. 6, 1968, pp. 815–822.

[63]Jameson, A., "Solution of the Euler Equations for 2-D Transonic Flow by a Multigrid Method," *Applied Mathematics and Computation*, Vol. 13, 1983, pp. 327–355.

[64]Leonard, B. P., "A Stable and Accurate Convective Modelling Procedure Based on Quadratic Upstream Interpolation," *Computational Methods in Applied Mechanics and Engineering*, Vol. 19, 1979, pp. 59–98.

[65]Ni, R. H., "A Multiple Grid Scheme for Solving the Euler Equations," *AIAA Journal*, Vol. 20, 1982, pp. 1565–1571.

[66]Lerat, A., "Implicit Methods of Two-Order Accuracy for the Euler Equations," *AIAA Journal*, Vol. 23, 1985, pp. 33–40.

[67]Lien, F. S., and Leschziner, M. A., "A General Nonorthogonal Collocated Finite Volume Algorithm for Turbulent Flow at All Speeds Incorporating Second-Moment Turbulence-Transport Closure—Part 1—Computational Implementation," *Computational Methods in Applied Mechanics and Engineering*, Vol. 114, 1994, pp. 123–148.

[68]Liu, F., and Jameson, A., "Multigrid Navier–Stokes Calculations for 3-D Cascades," *AIAA Journal*, Vol. 31, No. 10, 1993, pp. 1785–1791.

[69]Lax, P., and Wendroff, B., "Systems of Conservation Laws," *Communications on Pure and Applied Mathematics*, Vol. 13, 1960, pp. 217–237.

[70]Roe, P. L., "Approximate Riemann Solvers, Parameter Vectors and Difference Schemes," *Journal of Computational Physics*, Vol. 43, 1981, pp. 357–372.

[71]Roe, P. L., "Characteristic-Based Schemes for the Euler Equations," *Annual Review of Fluid Mechanics*, Vol. 18, 1986, pp. 337–365.

[72]Frink, N. T., "Upwind Scheme for Solving the Euler Equations on Unstructured Tetrahedral Meshes," *AIAA Journal*, Vol. 30, 1992, pp. 70–77.

[73]Yee, H. C., and Harten, A., "Implicit TVD Schemes for Hyperbolic Conservation Laws in Curvilinear Coordinates," *AIAA Journal*, Vol. 25, 1987, pp. 266–274.

[74]Van Leer, B., "Towards the Ultimate Conservative Difference Scheme. V. A 2-Order Sequel to Godunov's Method," *Journal of Computational Physics*, Vol. 32, 1979, pp. 101–136.

[75]Van Leer, B., "Flux-Vector-Splitting for the Euler Equations," *Lecture Notes in Physics*, Vol. 170, 1982, pp. 507–512.

[76]Anderson, W. K., Thomas, J. L., and Van Leer, B., "Comparison of Finite-Volume Flux-Vector-Splittings for the Euler Equations," *AIAA Journal*, Vol. 24, 1986, pp. 1453–1460.

[77]Anderson, W. K., Thomas, J. L., and Rumsey, C. L., "Extension and Application of Flux-Vector-Splitting to Calculations on Dynamic Meshes," *AIAA Journal*, Vol. 27, 1989, pp. 673–674; also AIAA Paper 87-1152.

[78]Rizzetta, D. P., and Visbal, M. R., "Comparative Numerical Study of Two Turbulence Models for Airfoil Static and Dynamic Stall," *AIAA Journal*, Vol. 31, 1993, pp. 784–786.

[79]Shih, S. H., Hamed, A., and Yeuan, J. J., "Unsteady Supersonic Cavity Flow Simulations Using Coupled k–ε and Navier–Stokes Equations," *AIAA Journal*, Vol. 32, No. 10, 1994, pp. 2015–2021.

[80]Jin, G., and Braza, M., "Two-Equation Turbulence Model for Unsteady Separated Flows Around Airfoils," *AIAA Journal*, Vol. 32, No. 12, 1994, pp. 2316–2320.

[81]Ekaterinaris, J. A., and Menter, F. R., "Computation of Oscillating Airfoil Flows with One- and Two-Equation Turbulence Models," *AIAA Journal*, Vol. 32, No. 12, 1994, pp. 2359–2365.

[82]Gerolymos, G. A., Vallet, I., Bölcs, A., and Ott, P., "Computation of Unsteady Three-Dimensional Transonic Nozzle Flows Using k–ε Turbulence Closure," *AIAA Journal*, Vol. 34, No. 7, 1996, pp. 1331–1340.

[83]Stüttgen, W., and Peters, N., "Stability of Similarity Solutions by Two-Equation Models of Turbulence," *AIAA Journal*, Vol. 25, 1987, pp. 824–830.

[84]Shih, T. I. P., and Chyu, W. J., "Approximate Factorization with Source Terms," *AIAA Journal*, Vol. 29, 1991, pp. 1759–1760.

[85]Favre, A., "Equations des Gaz Turbulents Compressibles. I. Formes Générales," *Journal de Mécanique*, Vol. 4, 1965, pp. 361–390.

[86]Favre, A., "Equations des Gaz Turbulents Compressibles. II. Méthode des Vitesses Moyennes; Méthode des Vitesses Moyennes Pondérées par la Masse Volumique," *Journal de Mécanique*, Vol. 4, 1965, pp. 391–421.

[87]Van Albada, G. D., Van Leer, B., and Roberts, W. W. Jr., "A Comparative Study of Computational Methods in Cosmic Gas Dynamics," *Astronomy and Astrophysics*, Vol. 108, 1982, pp. 76–84.

[88]Arnone, A., "Viscous Analysis of 3-D Rotor Flow using a Multigrid Method," *Journal of Turbomachinery*, Vol. 116, 1994, pp. 435–445.

[89]Vinokur, M., "An Analysis of Finite-Difference and Finite-Volume Formulations of Conservation Laws," *Journal of Computational Physics*, Vol. 81, 1989, pp. 1–52.

[90]Gerolymos, G. A., and Bréus, J. P., "Computation of Unsteady Nozzle Flow due to Fluctuating Back-Pressure Using Euler Equations," *Recherche Aérospatiale* (submitted for publication); also ASME Paper 94-GT-91.

[91]Golub, G. H., and Van Loan, C. F., *Matrix Computations*, Johns Hopkins Univ. Press, Baltimore, MD, 1989, pp. 150–152.

[92]Vallet, I., "Aérodynamique Numérique 3-D Instationnaire avec Fermeture Bas Reynolds au Second Ordre," Doctorat, Université Pierre-et-Marie-Curie, Paris, 1995.

[93]Raulot, A., "Modélisation et Calcul d'Ecoulements Transsoniques Turbulents à l'aide d'une Méthode Centrée sans Viscosité Artificielle," Doctorat, Université Pierre-et-Marie-Curie, Paris, 1994.

[94]Atkins, H., and Casper, J., "Nonreflective Boundary Conditions for High-Order Methods," *AIAA Journal*, Vol. 32, No. 3, 1994, pp. 512–518.

[95]Chakravarthy, S. R., "Euler Equations—Implicit Schemes and Boundary Conditions," *AIAA Journal*, Vol. 21, 1983, pp. 699–706.

[96]Gerolymos, G. A., Tsanga-Kepeden, G., and Vallet, I., "Computation of 3-D Transonic Cascade Flows Using k–ε Turbulence Closure" (manuscript in preparation).

[97]Délery, J. M., "Experimental Investigation of Turbulence Properties in Transonic Shock/Boundary-Layer Interactions," *AIAA Journal*, Vol. 21, 1983, pp. 180–185; also AIAA Paper 81-1245.

[98]Benay, R., Délery, J. M., and Pot, T., "Analyse Expérimentale de l'Ecoulement dans un Canal Transsonique 3-D," *Recherche Aérospatiale*, Vol. 1986, No. 6, 1986, pp. 399–414.

[99]Roache, P. J., "Perspective: A Method for Uniform Reporting of Grid Refinement Studies," *Journal of Fluids Engineering*, Vol. 116, 1994, pp. 405–413.

Color reproduction courtesy of Laboratoire d'Energétique, Université Pierre-et-Marie-Curie, Paris